Remote Sensing of Environment 113 (2009) 2412–2423

Contents lists available at ScienceDirect

Remote Sensing of Environment

journal homepage: www.elsevier.com/locate/rse

Mapping forest background reflectivit over North America with Multi-angle Imaging SpectroRadiometer (MISR) data

Jan Pisek [a,b,*], Jing M. Chen [a]

[a] University of Toronto, Department of Geography and Program in Planning, Sidney Smith Hall, 100 St. George Street, Room 5047, Toronto, ON, Canada M5S 3G3
[b] Tartu Observatory, 61602 Tõravere, Estonia

ARTICLE INFO

Article history:
Received 9 April 2009
Received in revised form 4 July 2009
Accepted 10 July 2009

Keywords:
Multi-angle remote sensing
MISR
Forest understory
LAI

ABSTRACT

The spatial and temporal patterns of the forest background optical properties are critically important in retrieving the biophysical parameters of the forest canopy (overstory) and in ecosystem modeling. In this paper we carry out background reflectivity mapping over conterminous United States, Canada, Mexico, and the Caribbean land mass using Multi-angle Imaging SpectroRadiometer (MISR) data at 1.1 km resolution. The refined methodology uses the nadir and 45° forward directions of the MISR camera images. The background reflectivity is shown to vary between coniferous and deciduous stands, particularly in the near-infrared band, and with the overall amount of overstory vegetation. The largest seasonal differences were observed over a boreal region. The main drawback is a high amount of missing MISR data due to the presence of clouds and other atmospheric effects. The paper also contains a demonstration of the effect on LAI estimates when the dynamic background reflectivity information is inserted into a global LAI algorithm. Multi-angular remote sensing is thus shown to enable us to effectively map yet another forest structure parameter over large areas, which was not possible using mono-angle data.

1. Introduction

Quantitative description of vegetation structure has been identified as one of the key requirements for major improvement in modeling the terrestrial carbon cycle and global biosphere (Turner et al., 2004). Vegetation canopy structure and its energy absorption capacity can be described by leaf area index (LAI), defined as half the total developed area of green leaves per unit ground horizontal area (Chen & Black, 1992) and by the Fraction of Photosyntetically Active Radiation (FAPAR) absorbed by the leaves. It was noted that for models of climate, hydrology, and ecology it is probable that only the LAI, FAPAR, and information about the forest floor albedo have to be estimated spatially (Diner et al., 2005). Other parameters can be derived from LAI or taken from the literature (Manninen & Stenberg, 2009).

While retrieving the information about forest vegetation structure such as LAI, it is the spectral signal from the forest canopy (overstory, see Fig. 1) that is the target in many remote sensing (RS) applications, and not the background. However, the sensor receives a signal from both the target and the background (Olofsson & Eklundh, 2007; Peltoniemi et al., 2005a). By the term forest background, we refer to all the materials below the forest canopy such as understory, leaf litter, grass, lichen, moss, rock, soil, snow, or their mixtures (Fig. 1).The stand is thus conceptually divided into tree canopy and background material + soil (Chopping et al., 2006).

The lack of spatial information about forest background and its importance has recently gained increased attention (e.g. Eriksson et al., 2006; Kuusk et al., 2004; Rautiainen, 2005). Particularly within relatively open forest canopies, understory vegetation, its contrasting greenness and senescence can be quite important to relationships between vegetation indices (VI) and overstory LAI (Pocewicz et al., 2007). Further, Garrigues et al. (2008) noted in their validation and intercomparison of global LAI products that the forest understory LAI is not systematically taken into account in ground LAI measurements. This can result in substantial differences with the satellite LAI product derived from the vertical integration of the radiometric signal within the canopy (Abuelgasim et al., 2006; Chen et al., 1997; Iiames et al., 2008; Wang et al., 2004). It is equally important to take the understory vegetation into account when measuring FAPAR, particularly in open canopies (Olofsson & Eklundh, 2007).

Driven by these calls, few efforts were carried out at collecting various understory components and/or creating limited spectral banks (Lang et al., 2002; Miller et al., 1997; Peltoniemi et al., 2005a,b; Rautiainen et al., 2007; Rees et al., 2004). Monitoring the environment at a continental or global scale over periods of multiple years requires access to continuous fields of geophysical quantities, and satellite RS is the only technology currently able to provide consistent data at these scales (Pinty et al., 2008). The information conveyed about canopy structure is small in the case of a mono-angle instrument, whose footprint does not spatially resolve individual scene elements

* Corresponding author. Tartu Observatory, 61602, Toravere, Tartumaa, Estonia.
E-mail address: jan.pisek@utoronto.ca (J. Pisek).

0034-4257/$ – see front matter © 2009 Elsevier Inc. All rights reserved.
doi:10.1016/j.rse.2009.07.003

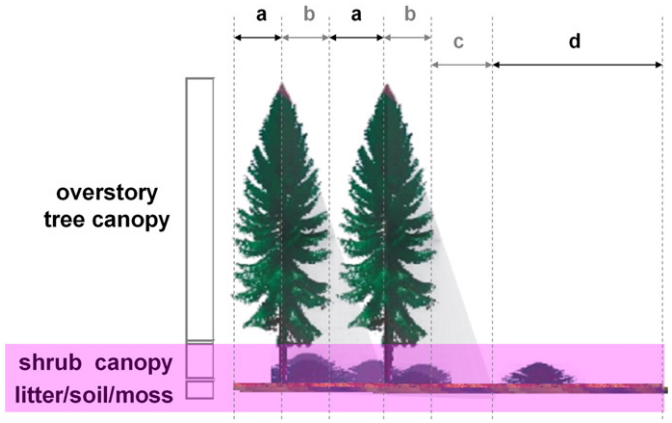

Fig. 1. Conceptual scheme of a forest stand. In vertical dimension the forest consists of overstory tree canopy; everything below (in purple) is considered to be the forest background. In horizontal dimension, the total reflectance of the stand is the sum of (a) sunlit tree, (b) shaded tree, (c) shaded ground, and (d) sunlit ground fractions. (For interpretation of the references to color in this figure legend, the reader is referred to the web version of this article.)

(Fig. 1). Therefore specifically in reference to LAI, a wide range of natural variation in LAI and soil or understory reflectance can result in the same value of the remotely sensed signal. This results in a high uncertainty in retrieved values of LAI (Hu et al., 2003). Before the era of simultaneously acquired multi-angle RS data by sensors such as MISR (Diner et al., 1998) or POLDER (Leroy & Lifermann, 2000) really started, Gemmell (2000) summarized that in the large majority of situations, the background spectral characteristics cannot be effectively obtained from the mono-angle RS data.

The use of multi-angle RS for characterizing surface properties represents a new paradigm in optical RS application (Nolin, 2004), where the variation in reflectance with view angle is considered a source of new information rather than noise. Multi-angle RS enables us now to describe surface properties by means that are not possible using mono-angle data (for a comprehensive review of the progress, see Chopping, 2008).

In this paper, we intend a) to document an improved retrieval strategy for the background reflectivity retrieval using geometrical optical modeling theory with the 4-Scale model and MISR data from the initial study published by Canisius and Chen (2007); b) to examine the optical properties and seasonal changes of the forest background over conterminous United States, Canada, Mexico and the Caribbean land mass over the year 2007; and c) to present on the example of the existing global LAI algorithms of Deng et al. (2006) a preliminary analysis of the effects of using the new background information dataset to correct the forest LAI estimates.

The improved strategy has been previously field-tested with multi-angle airborne Compact Airborne Spectrographic Imager (CASI) data (Pisek et al., 2009). The current paper presents, for the first time, a forest background dataset retrieved from MISR data at a continental scale and the implications for global LAI mapping.

2. Materials and methods

2.1. Background reflectivity algorithm

Since radiance is additive, the total spectral reflectance of a pixel (R) can be expressed as a linear combination of the contributions from the scene components (Bacour & Bréon, 2005; Chen et al., 2000; Chopping et al., 2008; Li & Strahler, 1985):

$$R = R_T \cdot k_T + R_G \cdot k_G + R_{ZT} \cdot k_{ZT} + R_{ZG} \cdot k_{ZG} \tag{1}$$

where R_T, R_G, R_{ZT}, and R_{ZG} are the reflectances of the sunlit tree crowns, sunlit background, shaded tree crown, and shaded background. k_j are the proportions of the four components in the instantaneous field of view (IFOV). By using the observed reflectance at nadir and at another angle one can derive the background reflectivity (R_G).

The first condition is that the observations are made along a plane where the target reflectances change little with view angle. The directional dependence of reflectance factors is the greatest in the principal solar plane and decreases fast as the viewing azimuth angle moves away from this plane (Bicheron et al., 1997; Peltoniemi et al., 2005b; Sandmeier & Deering, 1999). MISR is an operational sensor overpasssing the equator at approximately 10:30 local time while descending that provides high quality calibrated multi-angular measurements taken along an oblique plane, not so close to the principal plane (Diner et al., 2002). The influence of BRDF is then minimized and it has been observed that the azimuthal dependency of the reflectance of forest floor in particular is typically not that strong (Peltoniemi et al., 2005b) and forward-scattering reflectances of various targets were shown to be fairly constant (Bacour & Bréon, 2005; Deering et al., 1999; Kaasalainen & Rautiainen, 2005). The reflectance at nadir (n) and another zenith angle (a) can be then expressed by the Eqs. (2) and (3):

$$R_n = R_T \cdot k_{Tn} + R_G \cdot k_{Gn} + R_{ZT} \cdot k_{ZTn} + R_{ZG} \cdot k_{ZGn} \tag{2}$$

$$R_a = R_T \cdot k_{Ta} + R_G \cdot k_{Ga} + R_{ZT} \cdot k_{ZTa} + R_{ZG} \cdot k_{ZGa} \tag{3}$$

Canisius and Chen (2007) originally assumed the shaded reflectivities (i.e. R_{ZT} and R_{ZG}) to be comparatively small and replaced them by a constant value ($R_Z = R_{ZT} = R_{ZG}$) for individual wavelengths. However, Gemmell (2000) observed that reflectances from different shaded crowns could differ up to a factor or two. Pisek et al. (2009) tackled the issue in the new version of the algorithm (Eqs. (2) and (3) and used in this study for the first time with satellite RS data), by expressing shaded components of trees and ground dynamically as functions of their sunlit part and the multiple scattering factor (White et al., 2001, 2002a,b), giving $R_{ZT} = M \cdot R_T$ and $R_{ZG} = M \cdot R_G$, where $M = R_z / R$ for a reference target. Solving Eqs. (2) and (3), the background reflectivity R_G can be then calculated as:

$$R_G = \frac{R_n(k_{Ta} + k_{ZTa} \cdot M) - R_a(k_{ZTn} \cdot M)}{-k_{Tn} \cdot k_{Ga} + k_{Gn} \cdot k_{Ta} + M(-k_{Tn} \cdot k_{ZGa} + k_{Gn} \cdot k_{ZTa} - k_{Ga} \cdot k_{ZTn} + k_{Ta} \cdot k_{ZGn}) + M^2(-k_{ZTn} \cdot k_{ZGa} + k_{ZGn} \cdot k_{ZTa})} \tag{4}$$

where the total reflectances R_n and R_a are acquired from the nadir and chosen angle direction, M is predetermined by the 4-Scale model inversion, and the proportions of the components can be predicted from a GO model. We compare the performance of the algorithms by Canisius and Chen (2007) and Pisek et al. (2009) using MISR data in the Results section.

2.2. Estimating probabilities of viewing scene components

The proportions of the components in Eq. (4) are calculated using the 4-Scale model (Chen & Leblanc, 1997, 2001; Leblanc et al., 1999). This is a geometric–optical radiative-transfer model with an emphasis on the structural composition of forest canopies at different scales. From the model output, only the proportions of the components were used in the background reflectivity retrieval. The two most important properties of the 4-Scale from this point of view are:

a) Tree crowns are simulated as discrete geometrical objects: cone and cylinder for conifers, and spheroid for deciduous species, as this has been found to be an important parameter for correct BRDF model inversions (Rautiainen et al., 2004; 2008a). The non-random spatial distribution of trees is simulated using the Neyman type A distribution (Neyman, 1939).
b) The tree surface created by the crown volume is treated as a complex medium rather than a smooth surface so that shadowed foliage can be observed on the sunlit side and sunlit foliage on the shaded side.

Although the 4-Scale model requires many input parameters, it can be run with a fixed set of general parameters. Simulations by Nilson and Peterson (1994) pointed to the main factors in geometric–optical modeling of stand reflectances being LAI, canopy closure, tree type, and background reflectivity. Since according to their results parameters such as stand density, tree height, and tree stem diameter were not the most important factors, we used fixed values for these tree architectural parameters of coniferous and deciduous types as input to the 4-Scale model (Table 1). The parameters such as LAI, solar and view zenith angles (SZA and VZA), the relative azimuth angle between the sun and the viewing camera (PHI) varied between pixels. These parameters were obtained from the satellite images as described in the following section.

Running 4-Scale on multi-angle images pixel by pixel is computationally impractical with regard to the size of the assembled data. An alternative method of look-up tables (LUTs) has been previously applied for similar large dataset processing (Gobron et al., 2000; Myneni et al., 2002; Weiss et al., 2000). Ten LUTs, five for the coniferous and deciduous forest type each, were developed using the 4-Scale model. Ranges of values agree with the original LUT dimensions of Canisius and Chen (2007): LAI from 0.1 to 10, SZA from 0° to 70°, PHI from 100° to 170° along with the nominal VZA of MISR cameras. Despite advances in the retrieval of stand density from multi-angle RS (Heiskanen, 2006; Nolin, 2004), operational retrieval of the parameter over large areas is yet to be seen. However, the performance of the background reflectivity algorithm was shown not to be critically sensitive to the assumed stand density in case of low to intermediate densities (Pisek et al., 2009) when the influence of the background reflectance on the total canopy signal is the greatest (Rautiainen et al., 2007). The background reflectivity is thus calculated here as an average value of five results predicted with MISR data and multiple scattering factor M dependent on the wavelength while component fractions are retrieved from LUTs for five different stand densities for the given biome (Table 1).

2.3. MISR data and processing

The multi-angular satellite data were provided by MISR, which is onboard the Earth Observing System (EOS) satellite Terra (Diner et al., 1998, 2002). MISR consists of nine cameras; four point to the forward direction (denoted as AF, Bf, Cf, Df in the order of increasing off-nadir angle), one points towards the nadir (An) and four point to the aftward direction (Aa, Ba, Ca, Da). The nominal view angles of the cameras are 0°, ±26.1°, ±45.6°, ±60.0°, and ±70.5°. Each of the nine cameras obtains images at four spectral bands: blue (centered at 446 nm; bandwidth 42 nm), green (558 nm; 29 nm), red (672 nm, 22 nm) and near infrared (NIR) (866 nm; 40 nm) (Diner et al., 1998). MISR data employed in this study were acquired from all blocks arranged in orbits covering the North America in 2007. The data were provided by the Atmospheric Science Data Center (ASDC) at NASA Langley Research Center and ordered with the MISR Order Tool (2008).

A set of standard MISR data products is available, ranging from the raw instrument data to the calibrated and geolocated radiances, and geophysical retrievals of atmospheric and surface properties (Bothwell et al., 2002). MISR Level 2 products are resampled to 1.1 km resolution and are screened for contamination from sources such as clouds, cloud shadows, sun glitter over water, and topographically shadowed regions (Bothwell et al., 2002). MISR Level 2 MIL2ASLS Land Surface Parameters (surface bidirectional reflectance factor (BRF) and LAI), MISR Level 1B2 MI1B2GEOP Geometric Parameters (sun/view, zenith/azimuth angles), and MISR Ancillary Geographic Product (longitude and latitude of pixels) were used here.

MISR Level 2 products were provided in the Space Oblique Mercator (SOM) projection in equally sized blocks of an ellipsoidal surface defined by the World Geodetic System 1984 (WGS84). The block construct enables the co-registration of nine-angle, four-band images and allows stacking all the blocks of an orbit into a single dataset.

The MISR Level 2 Land Surface Product also includes biome information. Since Hu et al. (2003) observed incorrect assignment in 80% of pixels across five biomes, and serious misclassifications were noted in other papers as well (e.g. Pocewicz et al., 2007), we used the biome information

Table 1
Input parameters to 4-Scale.

Parameter	Unit	Coniferous	Deciduous
Stand density	Trees/ha	500, 1000, 2000 3000, 4000	500, 1000, 2000 3000, 4000
Clumping index (Ω_E)		0.7	0.8
Tree shape		Cone + cylinder	Spheroid
Crown base height	m	4	5
Crown vertical dimension	m	12	15
Crown radius (r)	m	0.75	2

from the GLC2000 dataset (Bartholomé & Belward, 2005; Loveland et al., 2000), instead. The same classification is used as an input into the global LAI algorithms of Deng et al. (2006) that are used later in the paper for the demonstration of the background reflectivity effect on LAI retrieval. Internal consistency between the two algorithm inputs (background reflectivity and LAI) is thus secured.

An IDL code was developed to read the data stored in stack-block and compute background reflectivity (R_G) from nadir and angular images. Canisius and Chen (2007) used 60° (Cf) camera for the angular information; 45.6° camera (Bf) is used in this paper. Previously, small co-registration errors were found for the Bf camera, but the revised algorithm fixed this and co-registration for all channels meets the expected goals now (Jovanovic et al., 2007). Smaller view angles than 60° are theoretically better due to the probability of observing larger proportions of background. Indeed, Pisek et al. (2009) observed slightly more accurate background reflectivity retrievals at smaller view zenith angles. These conclusions are also indirectly supported by findings of Rautiainen et al. (2008b), who noted that if the viewing azimuth angle is at the least 20° away from the principal plane (i.e. oblique plane), 56.7° view zenith angle is considerably more efficient than 37.2° in excluding the influence of the background especially in coniferous stands. The smaller view zenith angle also allows us to avoid the observed slight increase of BRF in the largest view angles in the forward-scattering direction in broadleaved species in particular, caused by the high canopy transmission and specular reflectance from the leaves (Deering et al., 1999).

The code was developed for a global application and automatically switches between forward and backward positioned cameras according to the value of PHI, as the scattering directions change with the sensor-sun configuration across the Earth. The background reflectivities were retrieved for the red and the NIR band and every orbit over North America in 2007. The orbit retrievals were then re-projected and combined into 10-day composite scenes in the Plate-Carree projection with the WGS84 coordinate system. The spatial and temporal interpolations, described below, were carried out on pixels within a latitude/longitude bounding box about the conterminous United States, Northern Canada, and the Caribbean landmass. The intent is to use a geographic domain of sufficient extent to illustrate the seasonal and regional variations while simultaneously restricting the computing time to a manageable level.

2.4. The spatial and temporal consistency

The global coverage time is 9 days for MISR (Diner et al., 2005), while the large-scale LAI algorithms produce results at around 10-day time steps (Baret et al., 2007; Fernandes et al., 2003; Myneni et al., 2002; Pisek et al., 2007). Fig. 2a,b shows the quantity and spatial coverage of retrieved background reflectivity values at 10-day time steps at the original MISR spatial resolution. Cloud contamination, persistent clouds, and other suboptimal atmospheric or illumination conditions can reduce the data quality and cause missing values in MISR Land Surface Products. About 20% of all forest pixels in the domain do not have a single successful retrieval; the percentage of pixels quickly drops with the number of retrieved background reflectivities. Additionally, the retrievals were not distributed evenly across the temporal domain, either.

Interpolation is essential under these conditions to reach continuous series free of missing data and of acceptable quality, as required by many climate modeling applications at the continental scale. Combination of spatial and temporal approaches offers superior interpolative capabilities to any single method, and in fact, generation of continuous data fields requires a hybrid approach such as this (Borak & Jasinski, 2009). The satisfactory temporal coverage, which enabled further temporal interpolation and reconstructing seasonal trajectories, was reached by upscaling the within one standard deviation background reflectivity retrievals to 1 decimal degree spatial resolution (Fig. 2c). Initial local window operations over the pixels with missing data, similar to the approach of Gao et al. (2008), with an automatic increasing of the spatial domain from 5×5 km/pixels in search of the successful retrievals were slow, prone to the outliers' bias and overall were not effective due to the occurrence of extensive areas of missing data.

Fig. 3 illustrates the consequent procedures of temporal interpolation and seasonal trajectories reconstruction with a series of moving temporal windows. The still missing data were replaced with the mean value of the observations recorded for that location in the preceding and the subsequent time period. A 5-value moving window was run next with the largest and the smallest value dropped before averaging. Finally, the monthly mean background reflectivity maps in the red and NIR band were produced.

2.5. Global LAI algorithms

Based on previous studies (Brown et al., 2000; Chen, 1996; Chen & Cihlar, 1997; Chen & Leblanc, 1997, 2001; Chen et al., 2002; Roujean et al., 1992), Deng et al. (2006) developed a set of LAI algorithms for the purpose of deriving global LAI products from multiple sensors. The algorithms are used for the production of the GLOBCARBON LAI product (Plummer et al., 2007). This set of algorithms has some unique features, including (a) explicit consideration of BRDF, (b) separate algorithms for several structurally distinct biomes, and (c) derivation of the effective rather than the true LAI from spectral indices. Deng et al. (2006) provide full accounts and theories for the algorithms used in this study. The input into the algorithms can also include background reflectivity data or vegetation clumping; if not specified, empirical values of background reflectivity and clumping index for different land cover types are used. Presence of an understory layer can substantially amplify the canopy LAI estimate (Chen et al., 1997; Eriksson et al., 2006) and it is an acknowledged source of uncertainty in global LAI modeling (Garrigues et al., 2008). Here, for the first time, we document the effect of using the derived MISR background reflectivity dataset on the output from the global LAI algorithms.

3. Results

3.1. Total and background reflectivity

The evaluation of effect of background on forest reflectance and the improvements of the background reflectivity algorithm are demonstrated first. As an example, we will now examine the retrievals covering path 21, orbit 18572 (mid-June) over Canada (Fig. 4). The orbit has been selected due to the excellent cloud-free conditions, a relatively high share of both deciduous and coniferous pixels (for each of the categories more than 15,000 pixels are reliable), and the coverage of the area of the original validation of the algorithm with in-situ spectral measurements and airborne CASI data (Pisek et al., 2009). The performance of the algorithm can be studied without the effect of later spatio-temporal interpolation and smoothing procedures, described in Section 2.3.

If the background reflectance signal did not differ from the overstory canopy, the understory effect on the canopy LAI retrievals would not be too high and could have been ignored. Fig. 5 illustrates the importance of not neglecting the background reflectivity on the example of coniferous forest. The plotted background reflectivities show non-negligible shifts in the spectral space from the total reflectances.

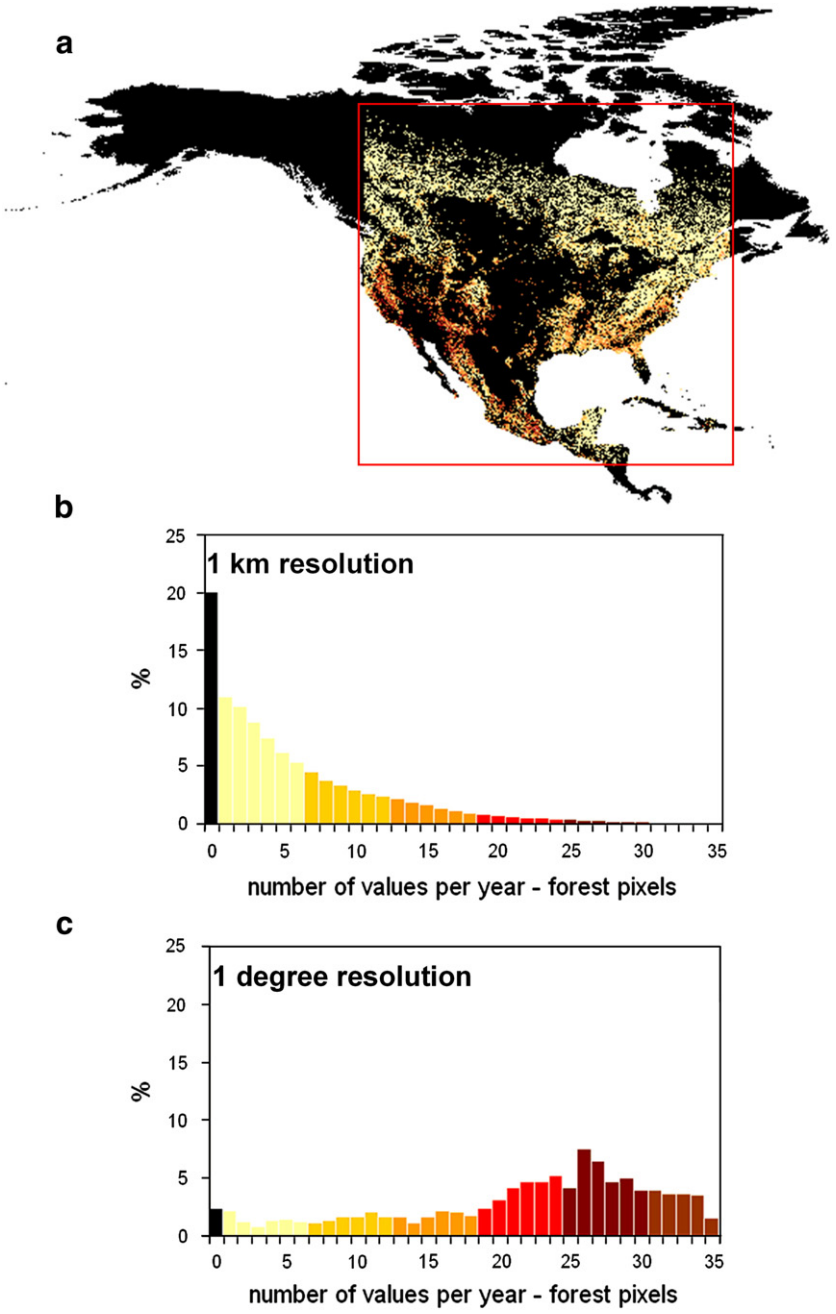

Fig. 2. (a) The spatial coverage and (b) quantity of retrieved forest background reflectivity values within the study area (red box) aggregated by 10-day time steps at original MISR spatial resolution of 1.1 km. (c) The distribution of values by the number of retrievals after aggregating the results to 1-degree resolution. (For interpretation of the references to color in this figure legend, the reader is referred to the web version of this article.)

The behavior is the same as the one observed by Pisek et al. (2009) with airborne data. The background reflectivities tend to be higher in both the red and the NIR band than the total reflectances. This is because the large shadow fractions at the stand level reduce the overall apparent reflectances from above the stand, while the background reflectivity refers to its inherent reflectivity.

3.2. Dynamic vs. constant shaded background reflectivities

Next, Table 2 offers a comparison of the retrievals to the ones using the algorithm of Canisius and Chen (2007) over the area in Fig. 4. The algorithms deliver slightly different frequency distribution of the results for both the coniferous and deciduous forest, particularly in the red band. The differences are the largest in case of deciduous forest, where the algorithm of Canisius and Chen (2007) predicts 62.3% of the reflectivities in the red band to be higher than 0.12 (Fig. 4b). This would indicate a presence of a very bright background such as snow (Peltoniemi et al., 2005b) in June. The algorithm of Canisius and Chen (2007) was originally developed for mapping over a limited area of boreal region only, with only a small fraction of deciduous forest. The variation of the background might have been then smaller and the constant shaded values corresponded to local conditions; results from Table 2 indicate this approach might not be optimal for a large-scale mapping. The current version with the non-constant shaded reflectivities places most of the values in the red band within the 0.04–0.08 reflectance interval (Fig. 4c), as would be expected at this time of the season.

The algorithm can occasionally predict negative background reflectivities that are screened out from the final results. Their share is not very high (maximum is 0.4% of retrievals over deciduous forest in

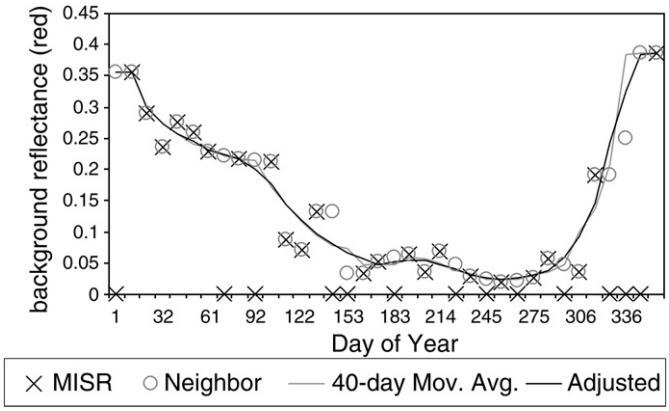

Fig. 3. Example of reconstructing seasonal-variation curves in the red band. Location of the sample area is 50° N, 77° W. The missing data were replaced first with the mean value (circles) of the valid observations (crosses) recorded in the preceding and subsequent time period. The smoothed values with a 40-day moving average window and the largest and the smallest values discarded before every averaging step (grey line); final monthly mean background reflectivity values (black line).

the sample area of Fig. 4; Table 2), but the break-down of negative retrievals by canopy LAI offers an insight into the role of overstory in the process (Table 3). The share of negative retrievals is increasing with canopy LAI in the case of deciduous forest, where a significant portion of the biome within the path area (Fig. 4a) does attain LAI>4. The higher amount of canopy LAI makes the understory more difficult to see from above, particularly from the slanted view angle. A high accuracy of the background retrievals for dense canopies is not possible due to this low visibility of the understory through the dense canopy. The stand reflectance at high LAI values is nearly independent of view directions, and as mentioned, the background has only a very small contribution to the total forest reflectance (Kaufmann et al., 2000; Zarco-Tejada et al., 2001; Zhang et al., 2002). If there is almost no visible understory, then there is no ability to measure background reflectivity. This inability results in the production of the negative values. The role of the background is not important then as well, as the background does not affect the total signal in case of these dense canopies (Lang et al., 2002; Olofsson & Eklundh, 2007). The dominant role of the spectral properties of understory compositions is at low canopy cover (Rautiainen et al., 2007), and the algorithm delivers stable results in this domain.

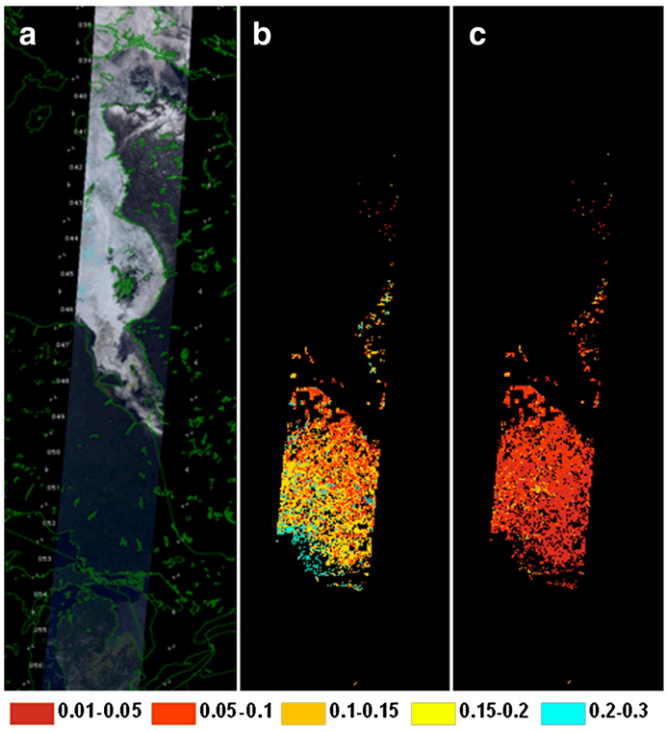

Fig. 4. (a) The coverage of MISR path 21, orbit 018572, over Ontario, Quebec, Hudson Bay and a part of Michigan. The MISR red, green and blue bands are used to create the color image, which has been clipped and gamma-stretched to make cloud, ocean and land features visible. Green lines refer to state/provincial boundaries and waterbody outlines (Original image a property of NASA Langley Research Atmospheric Sciences Data Center). Forest background reflectivity in the red band calculated with constant (b) and dynamic (c) reflectivities for the shaded fractions. (For interpretation of the references to color in this figure legend, the reader is referred to the web version of this article.)

3.3. Changing spectral properties of background with canopy LAI

The background spectral properties change with canopy openness, overall growing conditions, and the seasonal cycle (Fuller et al., 1997; Rautiainen et al., 2009). These variations can be observed in derived background reflectivities in June over both types of forest (Fig. 6). The range of values in the red and NIR band is quite wide for canopies with low LAI due to two reasons: first, high values in the red band and relatively low values in the NIR band correspond to surfaces with exposed bare soil and a minimum of vegetation cover, as the overall growing conditions are not favorable and result in low canopy LAI. Where the climatic and substrate growing conditions are more favorable to the understory vegetation, sufficient light can penetrate the overstory of open sites, and increasing amount of present understory vegetation lowers the reflectivity in the red band via higher absorption of chlorophylls and increases it in the NIR band, respectively (Haboudane et al., 2004; Nilson et al., 2003). It is at these extremely low coverages where the difficulties of canopy RS are the greatest due

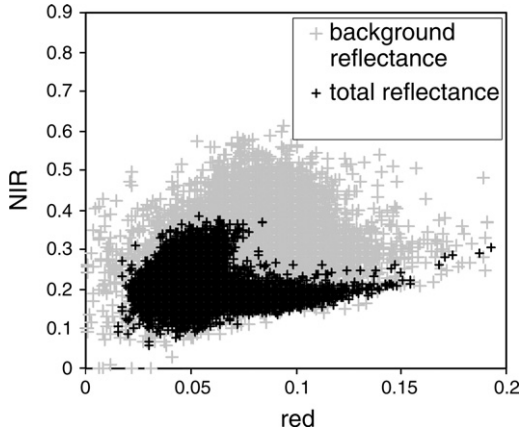

Fig. 5. Distribution of the total reflectance (black) and calculated background reflectivities (light grey) for coniferous forests over the parts of Ontario and Quebec in Fig. 4(a).

Table 2
Frequency of forest background reflectances in the red and the NIR bands over the area in Fig. 4, as predicted by the algorithm with dynamic and constant reflectances by shaded fractions.

	Forest	Coniferous		Deciduous	
	R_{ZT}, R_{ZG}	Dynamic	Constant	Dynamic	Constant
Band	BRF				
671.7 nm (red)	Less than zero	**0.1**	0.2	**0.2**	0.0
	0–0.019	0.2	0.2	1.0	0.0
	0.02–0.039	7.9	0.5	5.9	0.1
	0.04–0.059	36.1	6.7	23.4	1.8
	0.06–0.079	34.3	23.1	29.5	11.1
	0.08–0.099	16.2	33.6	18.5	14.0
	0.1–0.119	4.1	24.3	11.5	10.6
	>0.12	1.1	11.4	10.0	62.3
866.4 nm (NIR)	Less than zero	**0.0**	0.4	**0.4**	11.7
	0–0.09	0.1	0.5	1.1	2.1
	0.1–0.19	2.7	3.7	2.6	3.8
	0.2–0.29	27.9	16.9	8.7	7.5
	0.3–0.39	54.9	42.4	24.1	14.7
	0.4–0.49	13.8	30.0	37.5	21.7
	0.5–0.59	0.8	5.5	20.4	23.3
	>0.6	0.0	0.6	5.1	15.3

The break-down of the negative retrievals (in bold) is provided in Table 3.

to the overwhelming influence of soil and understory background on the spectral signature (DeFries et al., 2000). As the general growing conditions improve, both the canopy LAI and the amount of understory vegetation increase to the point where the decreasing amount of light transmitted through the overstory starts becoming a limiting factor (LAI = 3–4; Fig. 5). The amount of understory vegetation can start decreasing after this point and so does the reflectivity in the NIR band. The behavior in the red band seems to be slightly different between deciduous and coniferous stands at high LAI values (Fig. 6a, c). This may be a result of the observed greater aggregation of foliage in coniferous forests (Rautiainen & Stenberg, 2005), which permits more light to reach the understory layer. The degree of understory vegetation cover can be higher then in coniferous stands than in deciduous stands having the same LAI.

3.4. Differences in background reflectivity between coniferous and deciduous forests

Reflectances from coniferous and broadleaved trees differ significantly especially in the NIR band (Häme et al., 1997). Does the overall background reflectivity differ between coniferous and deciduous forests as well? Two background reflectivity sets at 1 decimal degree were created for June 2007, the first one by upscaling 1-km resolution retrievals over coniferous forest, the other one with deciduous forest only. There are no significant differences between the two forest backgrounds in the red band (Fig. 7). The retrieval differences are normally distributed around zero. The differences in the NIR band between the upscaled background reflectivities from the two biomes are normally distributed as well, but the coniferous forest background reflectance in NIR tends to have lower values than that of deciduous forest (Fig. 7). Our results are in line with field measurements of Goward et al. (1994), who observed higher NIR reflectance of broadleaf shrubs and herbs, such as sworn fern, big leaf maple, or blackberry, whereas moss and litter dominated under the coniferous forest.

Table 3
Distribution of negative forest background reflectances by the stand LAI over the area in Fig. 4.

BG BRF <0		0.1	0.0		0.2	0.4
	Coniferous			Deciduous		
LAI	Number of pixels	Red	NIR	Number of pixels	Red	NIR
0–1	24994	90 (0.4)	3 (0.0)	415		1 (0.2)
1–2	23972	3 (0.0)		6585		1 (0.0)
2–3	27302		2 (0.0)	2886		1 (0.0)
3–4	5567			3305		
4–5	484			1117	6 (0.5)	
5–6	246			1602	23 (1.4)	19 (1.2)
>6	7			277	3 (1.1)	39 (14.1)

Their percentage share on the total number of pixels in given LAI interval is in brackets.

3.5. Seasonal maps of forest background reflectivity

The seasonal changes of the forest background signal are best illustrated over the red band, as this wavelength region with low mean reflectance (e.g. the red spectral region around 672 nm) exhibits a relatively large reflectance variation compared to a high reflectance region with a rather small variation (e.g., the NIR region; Strub et al., 2003). Wide ranges of forest background reflectivities are present over the continent in January–March (Fig. 8). The presence of snow increases the foreground/background contrast in forest. The regions with very high red band reflectivities indicate the presence of the snow and the high values are close to the observed reflectances of snow by Miller et al. (1997) and Peltoniemi et al. (2005b). The southern parts of the continent are then characterized by lower reflectivities, corresponding to bare soil or understory vegetation. Melting of snow implies dramatic changes occurring at the forest floor (Pinty et al., 2008). This can be observed especially over Canada during the period from March to June (Fig. 8). The maps show the disappearance of the snow over the mid-west as well with the gradual transition to bare soil or low cover of the understory. The continental distribution is fairly stable during the main growing period from June to September, when both overstory and understory BRFs in the red band decrease over a large extent of the continent because of the high absorption by the chlorophylls as leaf area of canopy layers increases (Heiskanen, 2006). The picture starts to change again in October when the background reflectivity increases. This corresponds to the decay of absorbing chlorophylls and the beginning of the senescence period. By December a highly reflecting background covered by snow can be observed over most of the continent. The understory showed in this study exhibits vegetation indices that may be lower than but fall within a similar range of the overstory canopies, which are in agreement with the field studies by Goward et al. (1994) and Miller et al. (1997) over different parts of the United States and Canada.

3.6. Inclusion of the background reflectivity information in global LAI algorithms

These derived background reflectivity maps enable us to examine the realistic effect of forest background on LAI retrieval. The effect is illustrated with an example of an LAI map derived with the global LAI algorithm of Deng et al. (2006) and SPOT-VEGETATION satellite data over North America for June 2007. Two LAI maps were produced: the first one with the original version of the algorithms that uses constant background values corresponding to the bare soil (Fig. 9a), and another one where the dynamic forest background reflectivity retrievals from MISR were incorporated into the algorithm (Fig. 9b). The biggest difference between the two maps can be observed in a boreal region (Fig. 9c), where the background reflectivity information from MISR reduces the estimates of LAI by over 1. The reductions are in agreement with measured understory LAI in a boreal region e.g. by Sonnentag et al. (2007). The largest relative differences between the two LAI maps correspond to regions with low to intermediate canopy cover. Regions with higher canopy cover experience smaller reductions in LAI, as the influence of background reflectivity on total stand reflectance decreases. In addition, the understory vegetation might not be as abundant as well, as illustrated in Section 3.3. The reductions in LAI might not appear very large, yet the amounts correspond to the range of overestimations between various global LAI products and

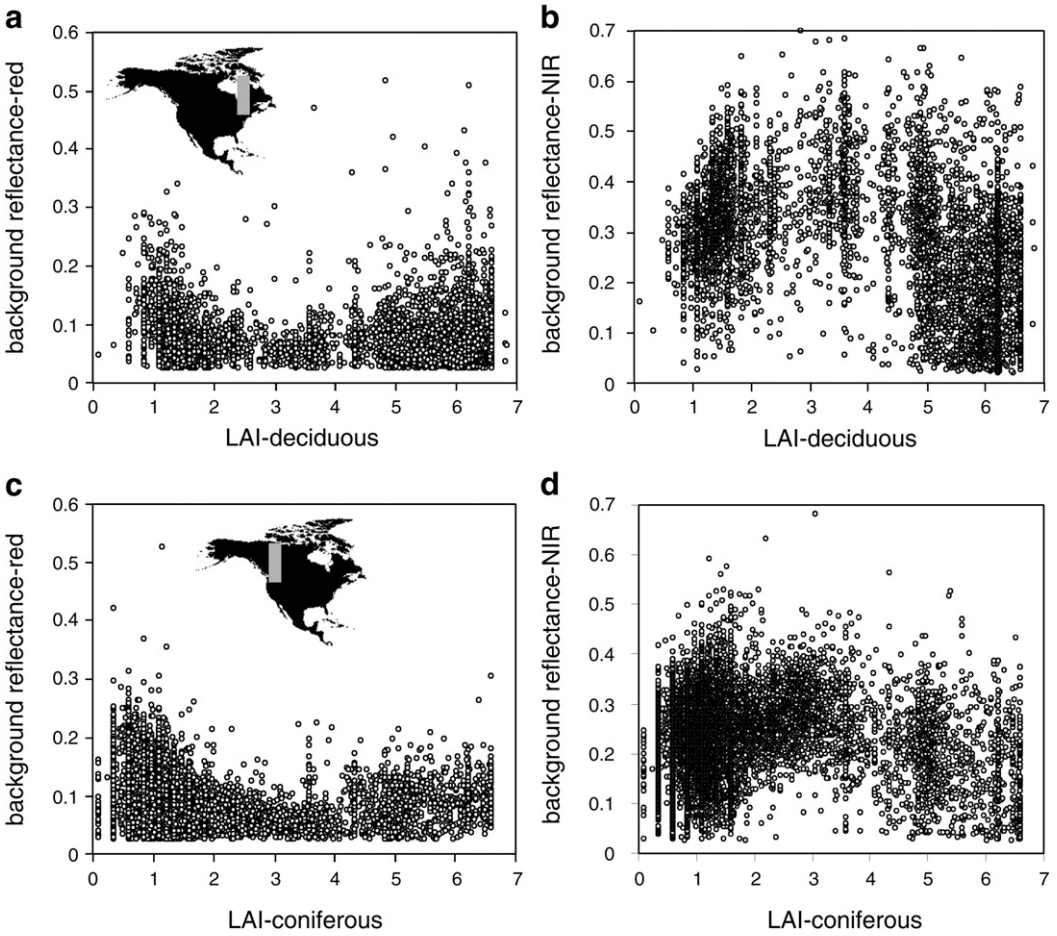

Fig. 6. The variations of background reflectivity with canopy LAI over the sample forested areas in Canada (grey boxes). (a) the red and (b) the NIR band, coniferous forest; (c) the red and (d) the NIR band, deciduous forest.

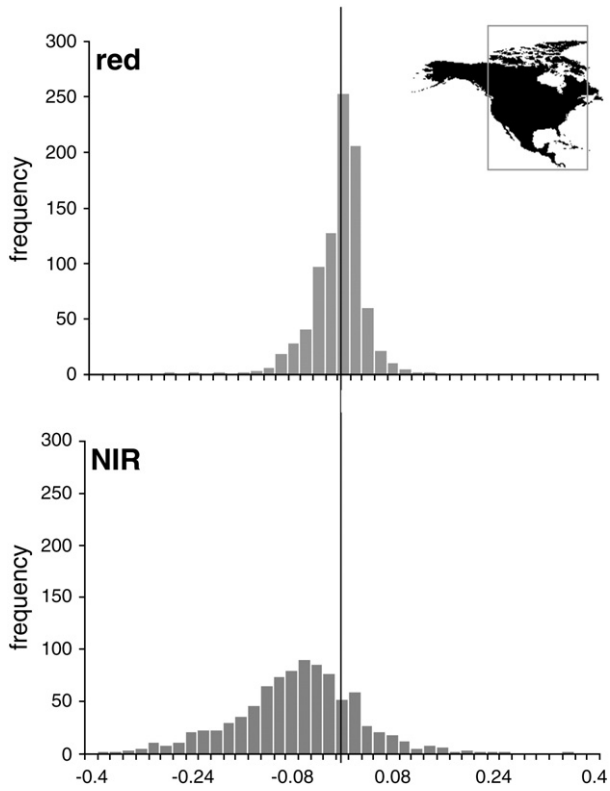

Fig. 7. Distribution of differences between the deciduous and coniferous forest background in the red and NIR bands if both types of forests were found within the corresponding 1-degree pixel. Negative values signify lower values for coniferous forest.

reference measurements over forest stands as observed by Garrigues et al. (2008). The dynamic background reflectivity maps from MISR thus definitely show the potential of filling the existing gap and might help us to bring the canopy LAI estimates from RS data in closer agreement with field observations.

4. Discussion

Given the rich content of multi-angular imagery, the analyses performed on the data have just begun to capitalize on the information provided by this measurement approach (Diner et al., 2005). The main reasons for the recent spark in the interest in forest understory are that the signal from the understory can be used, for example, (1) to remove the influence of understory in estimating canopy biophysical variables (e.g. LAI, FAPAR) from remotely sensed images (Garrigues et al., 2008), (2) to develop and test canopy radiative-transfer models (Widlowski et al., 2007), and (3) in forestry applications to separate forest site types (Rautiainen et al., 2009). In this study we demonstrate the applicability of the produced background reflectivity dataset to the first application.

It is encouraging to see the multi-angle view approach is capable of differentiating between different understory optical properties. However, separating understory cover components is not yet feasible, as the spectral properties of the individual species in the understory vegetation are generally similar, and the understory reflectance depends more on their abundance than on their spectral difference (Korpela, 2008; Peltoniemi et al., 2005a). For this task, a method of Rautiainen et al. (2007) with using visible bands of satellite images in sparse canopies or of Sonnentag et al. (2007) to account for a

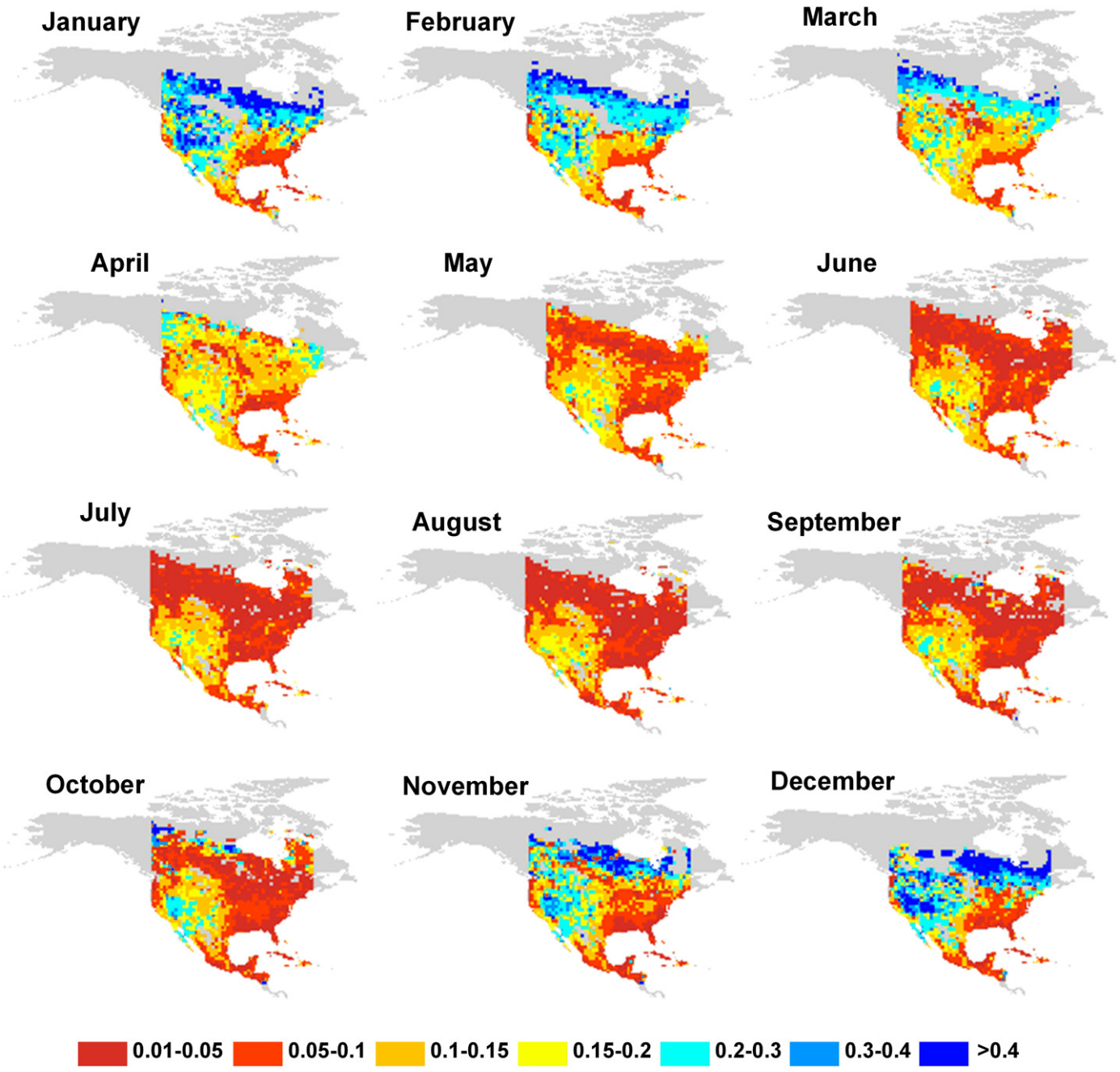

Fig. 8. Seasonal changes of the forest background reflectivity in the red band in 2007.

spectrally varying background using mixture signal decomposition might be more appropriate.

The rendering of the spring understory development sequence as shown in Fig. 8 would be useful for monitoring canopy phenology from satellite data such as MODIS (Ahl et al., 2006; Wang et al., 2005). As the canopy cover can be quite low in spring and the understory has been observed to start developing earlier than the overstory to take the advance of the light availability in the early growing season (Komiyama et al., 2001), the influence of the understory on the total signal and its variation can be quite significant especially during this season (Pocewicz et al., 2007).

The compilation of the background reflectivity dataset using MISR data also showed few drawbacks. First, in a marginal number of retrievals, the algorithm can predict negative reflectivity values. This is due to the effect of incorrect biome/initial LAI input information, or due to very low visibility of the understory through dense canopies which preclude a successful retrieval. However, the negative retrievals formed at maximum only 0.4% of all retrievals over the study area. Additionally, background has only a very small influence on LAI retrieval at high LAI values. Another drawback to be considered is the low resolution of the upscaled dataset tracking the seasonal development of the background reflectivity. Cloud contamination, persistent clouds, and other suboptimal atmospheric or illumination conditions caused significant swaths of missing values in the input MISR Surface Parameters data. However, the background in low and medium density forest stands is often similar within a geographical area (Kellomaki & Vaisanen, 1991; Muukkonen & Heiskanen, 2005; Reinikainen et al., 2001), although small scale variability may exist between stands of different densities in close proximity. As these coarse resolution background maps are mostly useful for low to medium density stands, this shortcoming of low resolution may be overcome in their application for regional and global LAI mapping. Furthermore, with respect to the

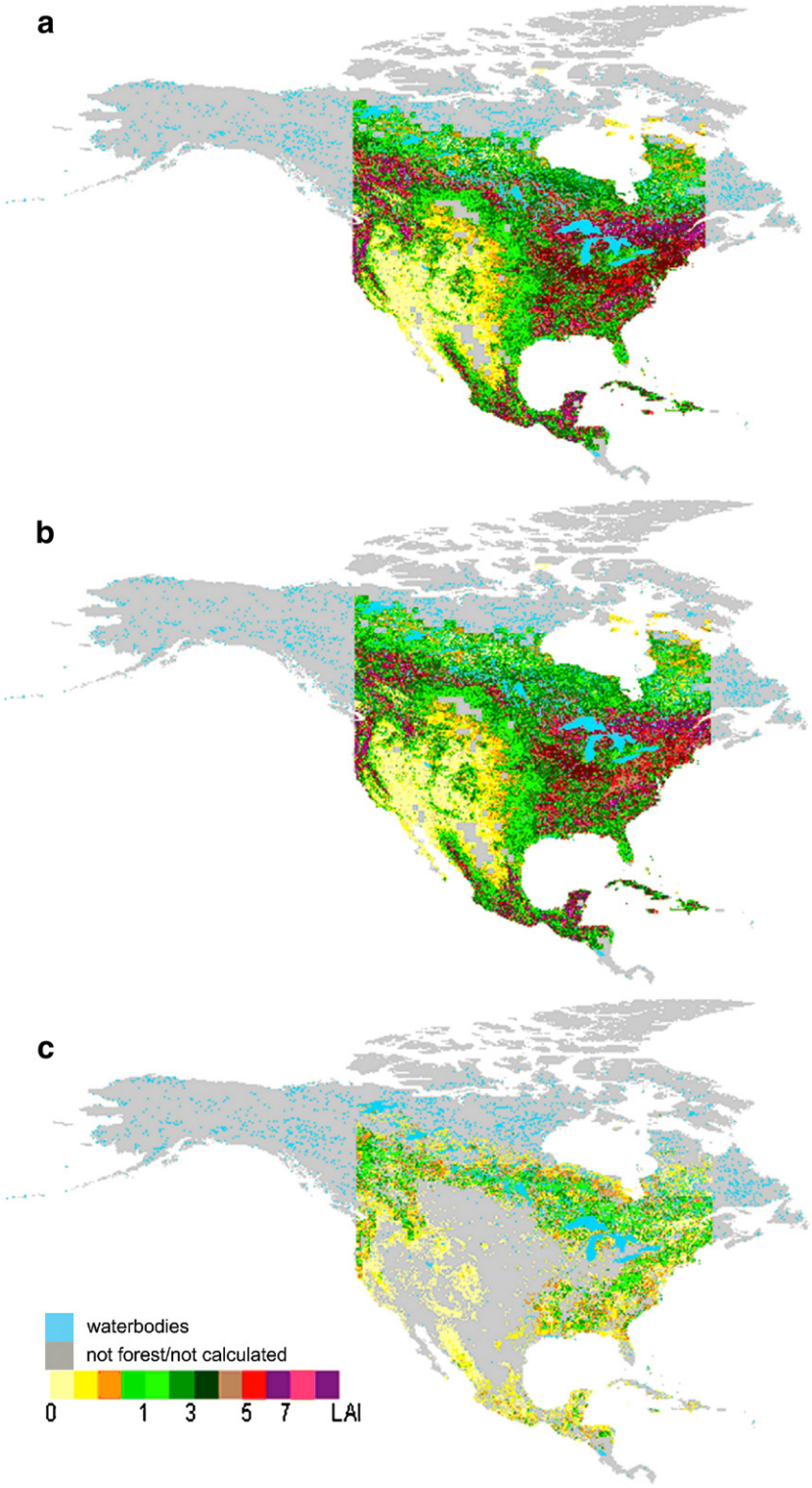

Fig. 9. Vegetation LAI fields over North America from the peak of boreal summer — July 2007. (a) constant forest background value for all pixels, (b) dynamic forest background from MISR data, (c) difference between the two maps over forest stands from MISR data.

mentioned application of the forest background information in canopy radiative-transfer and GO models, Kuusk et al. (2004) looked at the sensitivity of their hybrid type model to input understory parameters and they recommended using typical (average) parameter values while representing understory. Assembling multi-angle observations from multi-year time series of MISR data to fill in the missing areas could be an alternative strategy.

Unfortunately, we were unable to directly validate the derived background reflectivity values with measurement data. To our knowledge, there are currently no recorded, continuous measurements of the seasonal changes of spectral properties of understory layers. The general seasonal patterns and background spectral properties found in our study agree with the measurements done by e.g. Goward et al. (1994), Lang et al. (2002), Miller et al. (1997), Peltoniemi et al.

(2005a,b) or Pisek et al. (2009). This leads us to believe the observed temporal trends and spatial patterns are real.

5. Conclusions

In this study we demonstrate the capability of our refined approach and multi-angle RS data to retrieve meaningful background reflectivity information over large areas. For the first time, the forest background seasonal maps at a continental scale are presented here.

The retrieved background reflectivity shows the following characteristics:

(a) There are differences between the reflectances from the forest background and the total stand. This confirms that forest background cannot be ignored while retrieving canopy biophysical parameters from remotely sensed data. This is particularly true for stands with low canopy cover.
(b) Background reflectivity changes with the amount of canopy cover. This is primarily caused by the overall variation in the growth condition at different sites and the amount of light penetrating through the overstory.
(c) Forest background slightly differs between coniferous and deciduous stands, particularly in the NIR band. This may be linked to differences in prevailing understory species in these forest types.
(d) Significant seasonal development of the forest background vegetation can be observed across a wide longitudinal and latitudinal span of the study area.

The future work will focus on the full incorporation of the background vegetation values into global LAI algorithms. It remains to be seen if the information about the background helps us to reduce its effect on canopy LAI retrievals and improve the quality of various LAI products, a task much needed as suggested by Garrigues et al. (2008).

Acknowledgements

This study is supported by the Natural Science and Engineering Council of Canada (Discovery Grant) and a student assistantship to the first author by the Centre for Global Change Science at the University of Toronto. The MISR products were obtained from the NASA Langley Research Center Atmospheric Sciences Data Center. Leslie Erin Quinn and Thom Jones helped with English style corrections. We thank three anonymous reviewers who helped to improve this paper.

References

Abuelgasim, A., Fernandes, R. A., & Leblanc, S. G. (2006). Evaluation of national and global LAI products derived from optical remote sensing instruments over Canada. *IEEE Transactions on Geoscience and Remote Sensing*, *44*, 1872−1884.
Ahl, D. E., Gower, S. T., Burrows, S. N., Shabanow, N. V., Myneni, R. B., & Knyazikhim, Y. (2006). Monitoring spring canopy phenology of a deciduous broadleaf forest using MODIS. *Remote Sensing of Environment*, *104*, 88−95.
Bacour, C., & Bréon, F. M. (2005). Variability of biome reflectance directional signatures as seen by POLDER. *Remote Sensing of Environment*, *98*, 80−95.
Baret, F., Hagolle, O., Geiger, B., Bicheron, P., Miras, B., Huc, M., et al. (2007). LAI, fAPAR, and fCover CYCLOPES global products derived from VEGETATION Part 1: Principles of the algorithm. *Remote Sensing of Environment*, *110*, 275−286.
Bartholomé, E., & Belward, A. S. (2005). GLC2000: A new approach to global land cover mapping from Earth observation data. *International Journal of Remote Sensing*, *26*, 1959−1977.
Bicheron, P., Leroy, M., Hautecoeur, O., & Bréon, F. M. (1997). Enhanced discrimination of boreal forest covers with directional reflectances from the airborne polarization and directionality of Earth reflectances (POLDER) instrument. *Journal of Geophysical Research*, *102*, 29517−29528.
Borak, J., & Jasinski, M. (2009). Effective interpolation of incomplete satellite-derived leaf-area index time series for the continental United States. *Agricultural and Forest Meteorology*, *149*, 320−332.
Bothwell, G. W., Hansen, E. G., Vargo, R. E., & Miller, K. C. (2002). The Multiangle Imaging SpectroRadiometer science data system, its products, tools and performance. *IEEE Transactions on Geoscience and Remote Sensing*, *40*, 1467−1476.
Brown, L. J., Chen, J. M., Leblanc, S. G., & Cihlar, J. (2000). Short wave infrared correction to the simple ratio: An image and model analysis. *Remote Sensing of Environment*, *71*, 16−25.
Canisius, F., & Chen, J. (2007). Retrieving forest background reflectance in a boreal region from Multi-angle Imaging SpectroRadiometer (MISR) data. *Remote Sensing of Environment*, *107*, 312−321.
Chen, J. M. (1996). Optically-based methods for measuring seasonal variation in leaf area index of boreal conifer forests. *Agricultural and Forest Meteorology*, *80*, 135−163.
Chen, J. M., & Black, T. A. (1992). Defining leaf area index for non-flat leaves. *Plant Cell & Environment*, *15*, 421−429.
Chen, J. M., & Cihlar, J. (1997). A hotspot function in a simple bidirectional reflectance model for satellite applications. *Journal of Geophysical Research*, *102*, 25907−25913.
Chen, J. M., & Leblanc, S. G. (1997). A four-scale bidirectional reflectance model based on canopy architecture. *IEEE Transactions on Geoscience and Remote Sensing*, *35*, 1316−1337.
Chen, J. M., & Leblanc, S. G. (2001). Multiple-scattering scheme useful for geometric optical modeling. *IEEE Transactions on Geoscience and Remote Sensing*, *39*, 1061−1071.
Chen, J. M., Li, X., Nilson, T., & Strahler, A. (2000). Recent advances in geometrical optical modeling and its applications. *Remote Sensing Reviews*, *18*, 227−262.
Chen, J. M., Pavlic, G., Brown, L., Cihlar, J., Leblanc, S. G., White, H. P., et al. (2002). Validation of Canada-wide leaf area index maps using ground measurements and high and moderate resolution satellite imagery. *Remote Sensing of Environment*, *80*, 165−184.
Chen, J. M., Rich, P. M., Gower, T. S., Norman, J. M., & Plummer, S. (1997). Leaf area index of boreal forests: Theory, techniques and measurements. *Journal of Geophysical Research*, *102*, 29429−29444.
Chopping, M. (2008). Terrestrial applications of multiangle remote sensing. In S. Liang (Ed.), *Advances in Land Remote Sensing* (pp. 95−144). Spirnger Ch. 5.
Chopping, M., Moisen, G. G., Su, L. H., Laliberte, A., Rango, A., Martonchik, J. V., et al. (2008). Large area mapping of southwestern crown cover, canopy height, and biomass using the NASA Multiangle Imaging Spectro-Radiometer. *Remote Sensing of Environment*, *112*(5), 2051−2063.
Chopping, M., Su, L., Laliberte, A., Rango, A., Peters, D. P. C., et al. (2006). Mapping shrub abundance in desert grasslands using geometric–optical modeling and multiangle remote sensing with CHRIS/Proba. *Remote Sensing of Environment*, *104*, 62−73.
Deering, D. W., Eck, T. F., & Banerjee, B. (1999). Characterization of the reflectance anisotropy of three boreal forest canopies in spring–summer. *Remote Sensing of Environment*, *67*, 205−229.
DeFries, R., Hansen, M., Townshend, J. R. G., Janetos, A. C., & Loveland, T. R. (2000). A new global 1 km data set of percent tree cover derived from remote sensing. *Global Change Biology*, *6*, 247−254.
Deng, D., Chen, J. M., Plummer, S., Chen, M., & Pisek, J. (2006). Global LAI algorithm integrating the bidirectional information. *IEEE Transactions on Geoscience and Remote Sensing*, *44*, 2219−2229.
Diner, D. J., Beckert, J. C., Bothwell, G. W., & Rodriguez, J. I. (2002). Performance of the MISR instrument during its first 20 months in Earth orbit. *IEEE Transactions on Geoscience and Remote Sensing*, *40*, 1449−1466.
Diner, D. J., Beckert, J. C., Reilly, T. H., Bruegge, C. J., Conel, J. E., Kahn, R. A., et al. (1998). Multi-angle Imaging SpectroRadiometer (MISR) instrument description and experiment overview. *IEEE Transactions on Geoscience and Remote Sensing*, *36*, 1072−1087.
Diner, D. J., Braswell, B. H., Davies, R., Gobron, N., Hu, J., Jin, Y., et al. (2005). The value of multiangle measurements for retrieving structurally and radiatively consistent properties of clouds, aerosols, and surfaces. *Remote Sensing of Environment*, *97*, 495−518.
Eriksson, H., Eklundh, L., Kuusk, A., & Nilson, T. (2006). Impact of understory vegetation on forest canopy reflectance and remotely sensed LAI estimates. *Remote Sensing of Environment*, *103*, 408−418.
Fernandes, R. A., Butson, C., Leblanc, S., & Latifovic, R. (2003). Landsat-5 TM and Landsat-7 ETM+ based accuracy assessment of leaf area index products for Canada derived from SPOT4/VGT data. *Canadian Journal of Remote Sensing*, *29*, 241−258.
Fuller, D. O., Prince, S. D., & Astle, W. L. (1997). The influence of canopy strata on remotely sensed observations of savanna–woodlands. *International Journal of Remote Sensing*, *18*, 2985−3009.
Gao, F., Morisette, J. T., Wolfe, R. E., Ederer, G., Pedelty, J., Masuoka, E., et al. (2008). An algorithm to produce temporally and spatially continuous MODIS–LAI time series. *IEEE Geoscience and Remote Sensing Letters*, *5*, 60−64.
Garrigues, S., Lacaze, R., Baret, F., Morisette, J. T., Weiss, M., et al. (2008). Validation and intercomparison of global leaf area index products derived from remote sensing data. *Journal of Geophysical Research*, *113*. doi:10.1029/2007JG000635.
Gemmell, F. (2000). Testing the utility of multi-angle spectral data for reducing the effects of background spectral variations in forest reflectance model inversion. *Remote Sensing of Environment*, *72*, 46−63.
Gobron, N., Pinty, B., Verstraete, M., Martonchik, J., Knyazikhin, Y., & Diner, D. (2000). Potential of multiangular spectral measurements to characterize land surfaces: Conceptual approach and exploratory application. *Journal of Geophysical Research-Atmospheres*, *105*, 17539−17549.
Goward, S. N., Huemmrich, K. F., & Waring, R. H. (1994). Visible-near infrared spectral reflectance of landscape components in western Oregon. *Remote Sensing of Environment*, *47*, 190−203.
Haboudane, D., Miller, J. R., Pattey, E., Zarco-Tejada, P. J., & Strachan, I. B. (2004). Hyperspectral vegetation indices and novel algorithms for predicting green LAI of crop canopies: Modeling and validation in the context of precision agriculture. *Remote Sensing of Environment*, *90*, 337−352.
Häme, T., Salli, A., Andersson, K., & Lohi, A. (1997). A new methodology for the estimation of biomass of conifer-dominated boreal forest using NOAA AVHRR data. *International Journal of Remote Sensing*, *18*, 3211−3243.
Heiskanen, J. (2006). Tree cover and height estimation in the Fennoscandian tundra–taiga transition zone using multiangular MISR data. *Remote Sensing of Environment*, *103*, 97−114.

Hu, J., Tan, B., Shabanov, N. V., Crean, K. A., Martonchik, J. V., Diner, D. J., et al. (2003). Performance of the MISR LAI and FPAR algorithm: A case study in Africa. *Remote Sensing of Environment*, *88*, 324—340.

Iiames, J., Congalton, R., Pilant, A., & Lewis, T. (2008). Leaf area index (LAI) change detection analysis on Loblolly Pine (*Pinus taeda*) following complete understory removal. *Photogrammetric Engineering and Remote Sensing*, *74*, 1389—1400.

Jovanovic, V., Moroney, C., & Nelson, D. (2007). Multi-angle geometric processing for globally geo-located and co-registered MISR image data. *Remote Sensing of Environment*, *107*, 22—32.

Kaasalainen, S., & Rautiainen, M. (2005). Hot spot reflectance signatures of common boreal lichens. *Journal of Geophysical Research*, 110, D20102. doi:10.1029/2005JD005834.

Kaufmann, R. K., Zhou, L., Knyazikhin, Y., Shabanov, N. V., Myneni, R. B., & Tucker, C. J. (2000). Effect of orbital drift and sensor changes on the time series of AVHRR vegetation index data. *IEEE Transactions on Geoscience and Remote Sensing*, *38*, 2584—2597.

Kellomaki, S., & Vaisanen, H. (1991). Application of a gap model for the simulation of forest ground vegetation in boreal conditions. *Forest Ecology and Management*, *42*, 35—47.

Komiyama, A., Kato, S., & Teranishi, M. (2001). Differential overstory leaf flushing contributes to the formation of a patchy understory. *Journal of Forestry Research*, *6*, 163—171.

Korpela, I. (2008). Mapping of understory lichens with airborne discrete-return LiDAR data. *Remote Sensing of Environment*, *112*, 3891—3897.

Kuusk, A., Lang, M., & Nilson, T. (2004). Simulation of the reflectance of ground vegetation in sub-boreal forests. *Agricultural and Forest Meteorology*, *126*, 33—46.

Lang, M., Kuusk, A., Nilson, T., Lükk, T., Pehk, M., & Alm, G. (2002). *Reflectance spectra of ground vegetation in sub-boreal forests.* http://www.aai.ee/bgf/ger2600/index.html. Accessed September, 2008.

Leblanc, S. G., Bicheron, P., Chen, J. M., Leroy, M., & Cihlar, J. (1999). Investigation of directional reflectance in boreal forests with an improved 4-Scale model and airborne POLDER data. *IEEE Transaction on Geoscience and Remote Sensing*, *37*, 1396—1414.

Leroy, M., & Lifermann, A. (2000). The POLDER instrument onboard ADEOS: Scientific expectations and first results. *Advanced Space Research*, *25*, 947—952.

Li, X., & Strahler, A. (1985). Geometric-Optical modelling of a conifer forest canopy. *IEEE Transactions on Geoscience and Remote Sensing*, *23*, 207—221.

Loveland, T. R., Zhu, Z., Ohlen, D. O., Brown, J. F., Redd, B. C., & Yang, L. (2000). An analysis of the IGBP global land cover characterization process. *Photogrammetric Engineering and Remote Sensing*, *65*, 1021—1031.

Manninen, T., & Stenberg, P. (2009). Simulation of the effect of snow covered forest floor on the total forest albedo. *Agricultural and Forest Meteorology*, *149*, 303—319.

Miller, J., White, P., Chen, J., Peddle, D., McDemid, G., Fournier, R., et al. (1997). Seasonal change in the understory reflectance of boreal forests and influence on canopy vegetation indices. *Journal of Geophysical Research*, *102*, 29475—29482.

MISR Order Tool (2008). *NASA Langley Atmospheric Science Data Center.* http://l0dup05.larc.nasa.gov/MISR/cgi-bin/MISR/main.cgi/. Accessed October.

Muukkonen, P., & Heiskanen, J. (2005). Estimating biomass for boreal forests using ASTER satellite data combined with standwise forest inventory data. *Remote Sensing of Environment*, *99*, 434—447.

Myneni, R. B., Knyazikhin, Y., Privette, J. L., Glassy, J., Tian, Y., Wang, Y., et al. (2002). Global products of vegetation leaf area and fraction absorbed PAR from year one of MODIS data. *Remote Sensing of Environment*, *83*, 214—231.

Neyman, J. (1939). On a new class of "contagious" distributions applicable in entomology and bacteriology. *Annals of Mathematical Statistics*, *10*, 35—57.

Nilson, T., Kuusk, A., Lang, M., & Lükk, T. (2003). Forest reflectance modeling: Theoretical aspects and applications. *Ambio*, *32*, 535—541.

Nilson, T., & Peterson, U. (1994). Age dependence of forest reflectance: Analysis of main driving factors. *Remote Sensing of Environment*, *48*, 319—331.

Nolin, A. W. (2004). Towards retrieval of forest cover density over snow from the Multi-angle Imaging SpectroRadiometer (MISR). *Hydrological Processes*, *18*, 3623—3636.

Olofsson, P., & Eklundh, L. (2007). Estimation of absorbed PAR across Scandinavia from satellite measurements. Part II: Modeling and evaluating the fractional absorption. *Remote Sensing of Environment*, *110*, 240—251.

Peltoniemi, J. I., Kaasalainen, S., Näränen, J., Matikainen, L., & Piironen, J. (2005b). Measurement of directional and spectral signatures of light reflectance by snow. *IEEE Transactions on Geoscience and Remote Sensing*, *43*, 2294—2304.

Peltoniemi, J. I., Kaasalainen, S., Näränen, J., Rautiainen, M., Stenberg, P., Smolander, H., et al. (2005a). BRDF measurement of understory vegetation in pine forests: Dwarf shrubs, lichen, and moss. *Remote Sensing of Environment*, *94*, 343—354.

Pinty, B., Lavergne, T., Kaminski, T., Aussedat, O., Giering, R., Gobron, N., et al. (2008). Partitioning the solar radiant fluxes in forest canopies in the presence of snow. *Journal of Geophysical Research*, *113*. doi:10.1029/2007JD009096 D04104.

Pisek, J., Chen, J. M., & Deng, F. (2007). Assessment of a new global leaf area index dataset from SPOT-4 VEGETATION data over selected sites in Canada. *Canadian Journal of Remote Sensing*, *33*, 341—356.

Pisek, J., Chen, J. M., Miller, J. R., Freemantle, J. R., Peltoniemi, J. I., & Simic, A., (2009). Mapping forest background reflectance in a boreal region using multi-angle Compact Airborne Spectrographic Imager (CASI) data. *IEEE Transactions on Geoscience and Remote Sensing, 47.* doi:10.1109/TGRS.2009.2024756.

Plummer, S., Arino, O., Ranera, F., Tansey, K., Chen, J. M., et al. (2007). The GLOBCARBON initiative — Global biophysical products for terrestrial carbon studies. *IEEE International Symposium on Geoscience and Remote Sensing, Barcelona, Spain, July 23–27, 2007.*

Pocewicz, A., Vierling, L., Lentile, L., & Smith, R. (2007). View angle effects on relationships between MISR vegetation indices and leaf area index in a recently burned ponderosa pine forest. *Remote Sensing of Environment*, *107*, 322—333.

Rautiainen, M. (2005). Retrieval of leaf area index for a coniferous forest by inverting a forest reflectance model. *Remote Sensing of Environment*, *99*, 295—303.

Rautiainen, M., Mottus, M., Stenberg, P., & Ervasti, S. (2008a). Crown envelope shape measurements and models. *Silva Finnica*, *42*, 19—33.

Rautiainen, M., Lang, M., Mottus, M., Kuusk, A., Nilson, T., et al. (2008b). Multi-angular reflectance properties of a hemiboreal forest: An analysis using CHRIS PROBA data. *Remote Sensing of Environment*, *112*, 2627—2642.

Rautiainen, M., Nilson, T., & Lukk, T., (2009). Seasonal reflectance trends of hemiboreal birch forests. *Remote Sensing of Environment, 113*, 805–815.

Rautiainen, M., & Stenberg, P. (2005). Application of photon recollision probability in coniferous canopy reflectance simulations. *Remote Sensing of Environment*, *96*, 98—107.

Rautiainen, M., Stenberg, P., Nilson, T., & Kuusk, A. (2004). The effect of crown shape on the reflectance of coniferous stands. *Remote Sensing of Environment*, *89*, 41—52.

Rautiainen, M., Suomalainen, J., Mõttus, M., Stenberg, P., Voipio, P., Peltoniemi, J., et al. (2007). Coupling forest canopy and understory reflectance in the Arctic latitudes of Finland. *Remote Sensing of Environment*, *110*, 332—343.

Rees, W., Tutubalina, O., & Golubeva, E. (2004). Reflectance spectra of subarctic lichens between 400 and 2400 nm. *Remote Sensing of Environment*, *90*, 281—292.

Reinikainen, A., Makipaa, R., Vanha-Majamaa, I., & Hotanen, J. -P. (Eds.). (2001). *Kasvit muuttuvassa metsäluonnossa*: Helsinki' Finnish Forest Research Institute 384 pp. (in Finnish).

Roujean, J. L., Leroy, M., & Deschamps, P. Y. (1992). A bidirectional reflectance model of the earth's surface for the correction of remote sensing data. *Journal of Geophysical Research*, *97*, 20455—20468.

Sandmeier, S., & Deering, D. W. (1999). Structure analysis and classification of boreal forests using airborne hyperspectral BRDF data from ASAS. *Remote Sensing of Environment*, *69*, 281—295.

Sonnentag, O., Chen, J. M., Roberts, D. A., Talbot, J., Halligan, K. Q., & Govind, A. (2007). Mapping tree and shrub leaf area indices in an ombrotrophic peatland through multiple endmember spectral unmixing. *Remote Sensing of Environment*, *109*, 342—360.

Strub, G., Schaepman, M., Knyazikhin, Y., & Itten, K. (2003). Evaluation of spectro-directional alfalfa canopy data acquired during DAISEX'99. *IEEE Transactions on Geoscience and Remote Sensing*, *41*, 1034—1042.

Turner, D. P., Ollinger, S., & Kimball, J. (2004). Integrating remote sensing and ecosystem process models for landscape- to regional-scale analysis of the carbon cycle. *BioScience*, *54*, 573—584.

Wang, Q., Tenhunen, J., Dinh, N., Reichstein, M., Otieno, D., Granier, A., et al. (2005). Evaluation of seasonal variation of MODIS derived leaf area index at two European deciduous broadleaf forest sites. *Remote Sensing of Environment*, *96*, 475—484.

Wang, Y., Woodcock, C. E., Buermann, W., Stenberg, P., Voipio, P., Smolander, H., et al. (2004). Evaluation of the MODIS LAI algorithm at a coniferous forest site in Finland. *Remote Sensing of Environment*, *91*, 114—127.

Weiss, M., Baret, F., Myneni, R. B., Pragnere, A., & Knyazikhin, Y. (2000). Investigation of a model inversion technique for the estimation of crop characteristics from spectral and directional reflectance data. *Agronomie*, *20*, 3—22.

White, H. P., Miller, J. R., & Chen, J. M. (2002a). Four-scale linear model for anisotropic reflectance (FLAIR) for plant canopies—Part II: Validation and inversion with CASI, POLDER, and PARABOLA data at BOREAS. *IEEE Transactions on Geoscience and Remote Sensing*, *40*, 1038—1046.

White, P. H., Deguise, J., Schwartz, J., Hitchcock, R., & Staenz, K. (2002b). Defining shaded spectra by model inversion for spectral unmixing of hyperspectral datasets — Theory and preliminary application. *Proceedings of the International Geosci. and Remote Sens. Symposium (IGARSS) and 24th Canadian Symposium on Remote Sensing* (pp. 989—991).

White, P. H., Miller, J. R., & Chen, J. M. (2001). Four-scale linear model for anisotropic reflectance (FLAIR) for plant canopies—Part I: Model description and partial validation. *IEEE Transactions on Geoscience and Remote Sensing*, *39*, 1073—1083.

Widlowski, J. L., Taberner, M., Pinty, B., Bruniquel-Pinel, V., Disney, M., Fernandes, R., et al. (2007). The third RAdiation transfer Model Intercomparison (RAMI) exercise: Documenting progress in canopy reflectance models. *Journal of Geophysical Research-Atmospheres*, *112*, D09111. doi:10.1029/2006JD007821.

Zarco-Tejada, P. J., Miller, J. R., Noland, T. L., Mohammed, G. H., & Sampson, P. H. (2001). Scaling-up and model inversion methods with narrow-band optical indices for chlorophyll content estimation in closed forest canopies with hyperspectral data. *IEEE Transactions on Geoscience and Remote Sensing*, *39*, 1491—1507.

Zhang, Y., Shabanov, N., Knyazikhin, Y., & Myneni, R. B. (2002). Assessing the information content of multiangle satellite data for mapping biomes: II. Theory. *Remote Sensing of Environment*, *80*, 435—446.